XVI International Conference on Durability of Building Materials and Components
DBMC 2023, China
K.F. Li and D.P. Fang (Eds)

Monitoring Steel Rebar Corrosion-induced Cracking in ECC Cover by DOFS

E Chen[1], H. Ye[1] and S.S. Zhang[1]

[1] School of Civil and Hydraulic Engineering, Huazhong University of Science and Technology, Wuhan, China, chene@hust.edu.cn (Corresponding author)

Abstract. *Steel corrosion is the main threat to the durability of concrete structures, and the cracking or spalling of concrete cover caused by the expansion of corroded steel can largely accelerate the deterioration process. Engineered cementitious composites (ECCs), as one type of high-performance fiber-reinforced cementitious composites with high tensile ductility and excellent ability of crack width control, have a great potential to be able to improve the durability of structures under corrosive environment. Nevertheless, corrosion of steel rebar may still happen in ECC if aggressive agents depassivate the rebar; therefore, the relationship between the corrosion level and cracking degree in ECC cover is essential for accurately estimating the corrosion condition as well as service life of steel reinforced ECC structures. This study investigates the cracking process of ECC under accelerated steel corrosion implemented by impressed current, during which the distributed optical fiber sensors (DOFS) were employed both on the steel rebar surface and surface of ECC specimens to monitor the internal strain and surface strain generated by the corrosion expansion. The results show that DOFS provide an effective non-destructive tool for detecting the corrosion of steel rebar at early stage when the surface cracks in ECC are not visible.*

Keywords: *ECC, Rebar Corrosion, Corrosion Cracking, Distributed Optical Fiber Sensors.*

1 Introduction

Steel corrosion is one of the main causes of deterioration in the performance of reinforced concrete structures. A passive film is usually formed on the steel rebar in a strong alkaline environment provided by the concrete pore solution. When carbon dioxide and water enter, the pH value decreases and the passive film is destroyed, leading to corrosion of the reinforcing steel. In a chloride environment, when the chloride ion concentration reaches a threshold level, the passive film would also be destroyed, causing steel corrosion. The volume of corrosion products produced by reinforcing steel corrosion is several times the original steel volume, so circumferential tensile stress is generated in the concrete cover under the internal expansion of corrosion products. When the stress reaches concrete tensile strength, cracks will be induced. The generation of corrosion-induced cracks could aggravate the invasion of harmful substances, thereby accelerating the corrosion process. In addition, steel corrosion causes the loss of the bar's cross-section and degrades the bond properties, which threatens the safety of reinforced concrete structures.

To overcome the brittleness problem of concrete, Li and Leung (1992) proposed a design theory of Engineered Cementitious Composite (ECC) based on the principle of micromechanics and fracture mechanics. ECC exhibits strain-hardening property under uniaxial tension, and can control the crack width below 100μm by multiple cracking which can improve the durability of structures. A few previous studies (Sahmaran et al. 2008, Chen and Yang, 2019, Qiu et al. 2020)

have shown that ECC can supress corrosion-induced cracking propagation and resist cover spalling. This indicates the better durability of ECC, while a new question is raised that what the relationship between the corrosion level and ECC cracking degree is. An answer to this question is the basis of durability design of steel reinforced ECC (R/ECC). The present study investigated the corrosion-induced cracking process of ECC by conducting accelerated corrosion tests. Distributed optical fiber sensors (DOFS) based on Optical Frequency Domain Reflectometer (OFDR) and Rayleigh scattering were used to monitor the strain of ECC surface and strain on the rebar surface. The obtained results can be used to calibrate the theoretical relation between corrosion level and the strain or cracking level of ECC, and can also provide a basis for developing non-destructive assessment of rebar corrosion state in R/ECC.

2 Experimental Description

2.1 Specimens Preparation

2.1.1 ECC

The raw materials of ECC adopted in this study included ordinary Portland cement with a cement grade of 42.5, domestic PVA fibers (with a diameter of 40μm, a length of 12mm, and a tensile strength of 1560MPa), polycarboxylate superplasticizer, quartz sand with a particle size range of 0.1-0.25mm, and class F fly ash with a particle size of 1250 mesh. The mix proportion is shown in Table 1. Five ECC dumbbell specimens were cast. The dumbbell specimens had the geometry shown in Fig. 1 and they were used for testing the tensile behavior of ECC. To induce corrosion in a short time, sodium chloride with a total mass fraction of 5% was added to the ECC mix.

Table1. Mix design of ECC (kg/m^3)

Cement	Fly ash	Sand	Water	SP	PVA	NaCl
277.74	1110.94	277.74	305.51	2.08	26	100

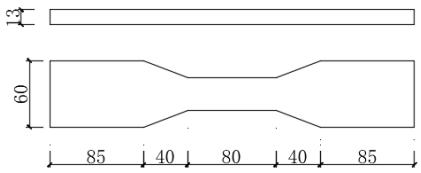

Figure 1. ECC dumbbell specimen size (unit in mm).

The specimens were demolded after 24 hours, and then cured in a standard environment with a temperature of 20±2°C and a relative humidity greater than 95%. After 28 days curing, uniaxial tensile tests were carried out. The loading rate was 0.2mm / min. An LVDT was placed on one side of the specimen to measure the total deformation within the 80 mm length in the middle of the specimen. The tensile test set-up is shown in Fig. 2.

Figure 2. ECC tensile test set-up.

2.1.2 Steel reinforced ECC cylinders

Two steel reinforced ECC cylinders were prepared, one embeeded with a smooth bar in the middle and the other one with a ribbed bar in the middle. They are denoted as smooth-R/ECC and ribbed-R/ECC respectively. The bar diameter is 16mm, and the cyclinder is 100 mm in diameter and 200 mm in height. The regions of steel bar located at the bottom and top ends of the cylinder were coated with epoxy to avoid pitting corrosion there. Before casting, the surface of the steel bar was spirally glued with a type of DOFS with sheathed protective layer and 0.9mm in diameter. After curing for 28 days, the surface of the cyclinder specimens were also spirally glued with a fiber sensor. The winding distance of the fiber sensor was about 40mm. The detailed size of the cylinder specimen and DOFS arrangement are shown in Fig. 3.

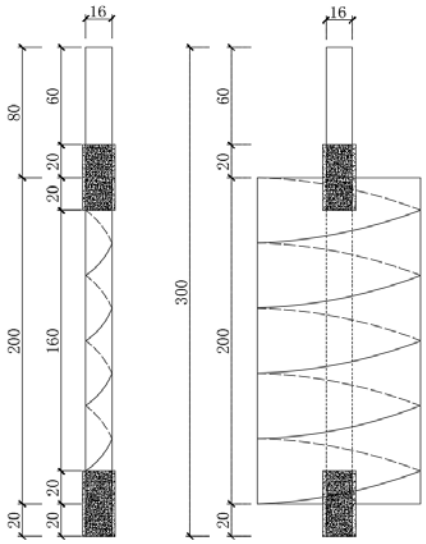

Figure 3. Sketch of the cylinder specimen and DOFS arrangement (unit in mm).

2.2 Accelerated Corrosion Test

To accelerate the corrosion process, impressed current method was used. Before applying the current, the specimens were immersed in water for 12 hours. The corrosion test set-up is shown in Fig. 4. The positive electrode of the power supply was connected to the steel bar, and the

negative electrode was connected to the stainless-steel mesh. A constant current applied to the specimen was set as 0.03 A. This corresponding to the corrosion current density of 373μA/cm^2 for the specimens in this study. The specimen ribbed-R/ECC was impressed current at the age of 29 days for about 25 hours, and then was placed in a natural state due to the Covid-19. The formal corrosion test was started at the age of 89 days. The specimen smooth-R/ECC was impressed current at the age of 120 days. After the accelerated corrosion test, the specimen was cut into thin slices for observing the internal crack pattern and corrosion distribution.

Figure 4. Accelerated corrosion test set-up and DOFS system.

3 Results and Discussions

3.1 Results of ECC Tensile Tests

All the dumbbell specimens exhibited multiple cracking during the tensile loading, as shown in Fig. 5a. The stress-strain curves of the five ECC specimens are shown in Fig.5b. Good ductility was obtained in these specimens.

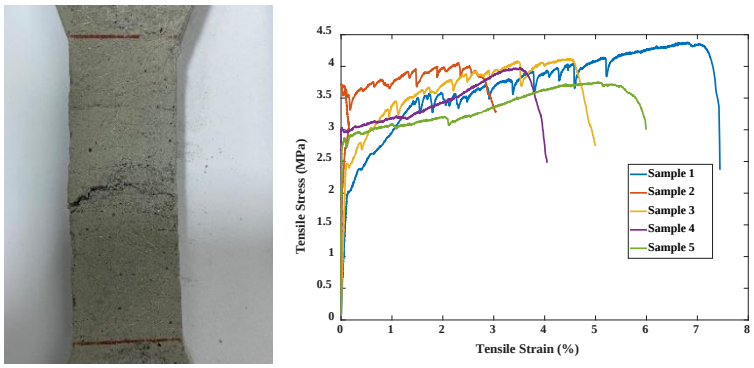

Figure 5. (a) Multiple-cracking in ECC under tension; (b) Tensile stress-strain curve of ECC.

3.2 Results of Accelerated Corrosion Tests

3.2.1 Corrosion-induced Strain Monitored by DOFS

During the corrosion test, the strain at the outer surface of the cylinder and interface between the steel bar and ECC was continuously monitored by DOFS. Figures 6 and 7 show the DOFS results for the two cylinders at different selected corrosion levels. The corrosion level labelled in Figs. 6 and 7 was theoretically calculated from Faraday's law:

$$\Delta m = \frac{WIt}{Fn} \tag{1}$$

where Δm represents the corrosion mass loss, W is the molar mass of iron (55.8g/mol), I is the current intensity (373 μA/cm^2), t represents the corrosion time, F is the Faraday constant (96500 coulombs), and n is the absolute value of total valence (taken as 2). The corrosion time was taken from the moment of current application. It should be noted that the real corrosion process might have started from casting of ECC, as chloride was present in the mix. This will be discussed later. The corresponding corrosion depth was also labelled in Figs. 6 and 7. The theoretical corrosion level and corrosion depth causing the corresponding strain level were much smaller than expected (which was estimated from the theory of elasticity). This is because the corrosion amount accumulated before the current application was not accounted for.

The reference strain of DOFS was recorded at the moment of starting the current apply. The strains measured by the DOFS on the rebar surface have more and more abnormal values at corrosion levels higher than about 1.5%, so only the results below this corrosion level are shown in Figs. 6 and 7 for the internal strains. The abormal results were mainly due to the strain gradient caused by cracking and exceedance of the maximum range of the DOFS. From Figs. 6 and 7, it is obviously seen that the strain distribution is different on the rebar surface and ECC surface. The internal strain distribution is nearly uniform while the strain on the outer surface has several high peaks. These peaks correspond to the corrosion-induced cracks. On the specimen surface, strain outside the cracks was much smaller than the peak strains. The more flat curves for the strain distribution at the rebar surface suggest that the internal cracks are more uniform than the outer surface.

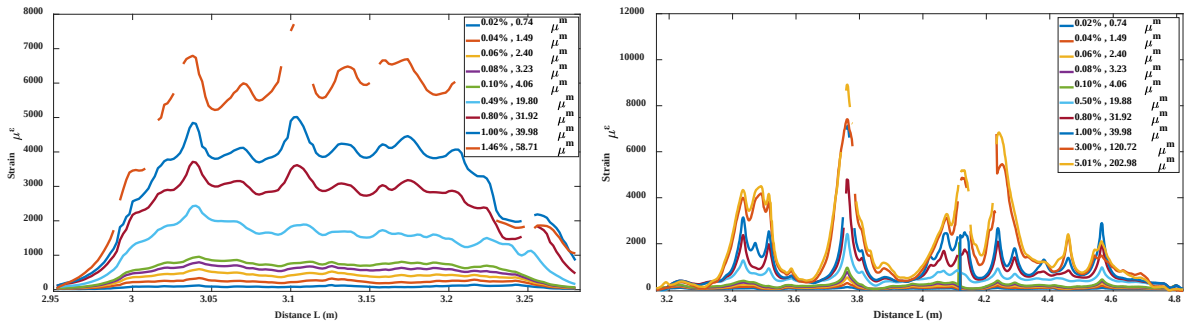

Figure 6. DOFS strains on the rebar surface and ECC surface at selected corrosion levels for the smooth-R/ECC specimen.

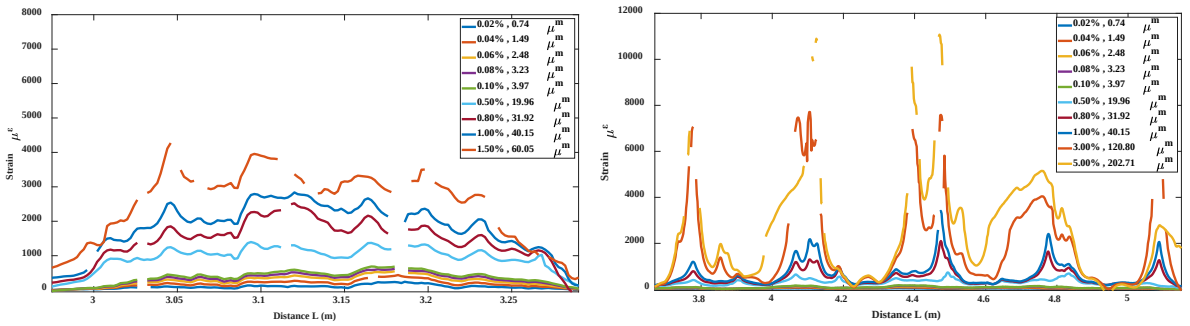

Figure 7. DOFS strains on the rebar surface and ECC surface at selected corrosion levels for the ribbed-R/ECC specimen.

To observe the strain distribution in the early stage, the DOFS results at selected early corrosion times are plotted in Figs. 8 and 9. It can be seen that the average strains at the rebar-ECC interface are greater than those at the outer surface, which is reasonable from the theory of elasticity. By comparing the strain distributions of the two specimens, it is found that the strain distribution and strain values are a little different for the smooth-R/ECC specimen and ribbed-R/ECC specimen at the same theoretical corrosion level.

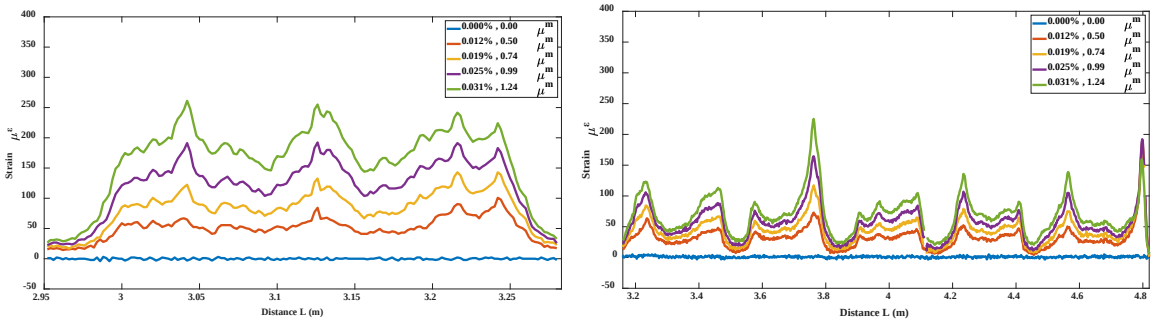

Figure 8. DOFS strains on the rebar surface and ECC surface at small corrosion levels for the smooth-R/ECC specimen.

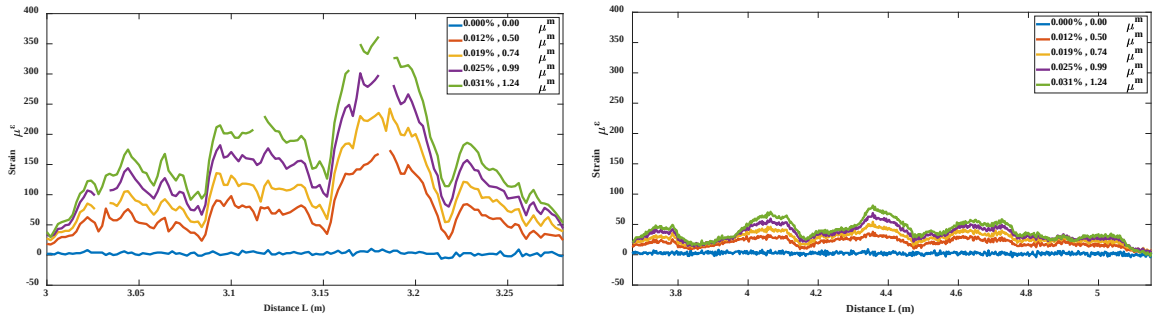

Figure 9. DOFS strains on the rebar surface and ECC surface at small corrosion levels for the ribbed-R/ECC specimen.

3.3 Cracking Pattern

The two specimens were cut into several slices to observe the internal crack pattern and corrosion distribution. The smooth-R/ECC specimen was cut by a thick cutter at first. It was found that the surface of the slices was not well flat and the edges of the steel surface was damaged a little. Therefore, a more precise and thinner cutter was used to cut the ribbed-R/ECC specimen. Before cutting on the precise cutter, the out portion of the ribbed-R/ECC specimen was cut off by the thick cutter first so that it can be placed on the thinner cutter set-up. Figure 10 shows that several corrosion-induced cracks were produced under the corrosion expansion. In normal concrete, the corrosion-induced cracks is usually localized into fewer major cracks.

Through the microscope observation, it was found that the fiber sensor was adhered on the smooth surface tightly while the fiber sensor was not directly attached on the rebar surface at some locations due to the transverse ribs, see Fig. 11. Therefore, the strain measured by the DOFS attached on the ribbed rebar may be a little different with the theoretical strain calculated right on the rebar surface from the classical corrosion expansion cylinder model. Further quantification analysis of the correlation between the corrosion-induced strain measured by DOFS and corrosion level should account for this.

Figure 10. Crack pattern in the smooth-R/ECC (left) and ribbed-R/ECC (right).

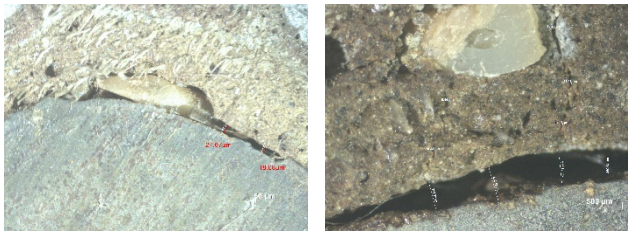

Figure 11. Fiber sensor at the smooth bar surface (left) and at the ribbed bar surface (right).

3.4 Steel Mass Loss

The total accelerated corrosion time of smooth-R/ECC specimen and ribbed-R/ECC specimen was 421 hours and 403 hours respectively, and the theoretical values of corrosion level of steel bar are 5.23 % and 5.01 % respectively. After the microscopic observation, the rebar segments were taken out. They were first sandblasted to remove the rust and then weighted. The results are given in Tables 3 and 4.

Table 3. Length and weight of slices of the smooth-R/ECC cylinder

	A-1	A-2	A-3	A-4	A-5	A-6	A-7	Total
Weight (g)	20.52	19.79	23.28	20.97	20.78	19.15	21.55	146.04
Length (mm)	13.9	13.5	15.8	14.1	14.0	13.2	14.8	99.3
Weight / Length	1.476	1.466	1.473	1.487	1.484	1.451	1.456	1.471

Table 4. Length and weight of slices of the ribbed-R/ECC cylinder

	B-1	B-2	B-3	B-4	B-5	Total
Weight (g)	28.07	20.2	19.81	21.22	21.06	110.36
Length (mm)	19.9	14.0	13.8	15.1	15.0	77.8
Weight / Length	1.411	1.443	1.436	1.405	1.404	1.419

From Tables 3 and 4, the actual corrosion level of specimens A and B are calculated as 5.73% and 5.64%. They are larger than the theoretical corrosion level calculated from Faraday's law. The reason is because of the natural corrosion before the current apply as mentioned. However, it was not possible to find the real corrosion amount under natural state in this study. To further correlate the corrosion level quantitatively with the corrosion-induced strain, it is better not to add chloride into the mix in order to remove the influence of the corrosion degree during the curing period.

4 Conclusions

The corrosion-induced cracking process in ECC with smooth and ribbed rebar was monitored by DOFS in this study. From this preliminary study, the following conclusions were obtained:

- DOFS can detect the early corrosion process by monitoring the corrosion-induced strain. However, the corrosion level calculated from Faradays' law to reach a certain corrosion-induced strain was smaller than expected because the actual corrosion level was larger.
- The strain on the rebar surface was more uniform than the strain on the ECC surface. In addition, the DOFS on the rebar surface failed to give reliable strain values at earlier stage, and the DOFS at the ECC surface could work at high corrosion levels.

References

Li V. C., Leung C. K. (1992). *Steady-state and multiple cracking of short random fiber composites*, Journal of Engineering Mechanics, 118(11), 2246-2264.

Sahmaran M, Li V C, Andrade C. (2008). *Corrosion Resistance Performance of Steel-Reinforced Engineered Cementitious Composite Beams,* ACI Materials Journal, 105(3):243-250.

Chen Z, Yang E. *Microstructural investigation of steel corrosion in strain hardening cementitious composite (SHCC),* Construction and Building Materials, 2019,211:185-198.

Qiu Q., Zhu J., Dai J. G. (2020). *In-situ X-ray microcomputed tomography monitoring of steel corrosion in engineered cementitious composite (ECC),* Construction and Building Materials, 262, 120844.